Global, high-resolution, reduced-complexity air quality modeling using InMAP (Intervention Model for Air Pollution)

Sumil K. Thakrar[1,2], Christopher W. Tessum[3], Joshua S. Apte[4,5], Srinidhi Balasubramanian[1], Dylan B. Millet[6], Spyros N. Pandis[7,8], Julian D. Marshall[9], Jason D. Hill[1*].

[1]Department of Bioproducts & Biosystems Engineering, University of Minnesota, St Paul, MN, USA.

[2]Department of Applied Economics, University of Minnesota, St Paul, MN, USA.

[3]Department of Civil and Environmental Engineering, University of Illinois at Urbana–Champaign, Urbana, IL, USA.

[4]Department of Civil and Environmental Engineering, University of California, Berkeley, Berkeley, CA, USA.

[5]School of Public Health, University of California, Berkeley, Berkeley, CA, USA.

[6]Department of Soil, Water, and Climate, University of Minnesota, St Paul, MN, USA.

[7]Department of Chemical Engineering, Carnegie Mellon University, Pittsburgh, PA, USA.

[8]Department of Chemical Engineering, University of Patras, Patras, Greece.

[9]Department of Civil and Environmental Engineering, University of Washington, Seattle, WA, USA.

Corresponding author: Jason D. Hill

Email: hill0408@umn.edu

ORCIDs:

Sumil K. Thakrar:	0000-0003-2205-3333
Christopher W. Tessum:	0000-0002-8864-7436
Joshua S. Apte:	0000-0002-2796-3478
Srinidhi Balasubramanian:	0000-0002-6561-5984
Dylan B. Millet:	0000-0003-3076-125X
Spyros N. Pandis	0000-0001-8085-9795
Julian D. Marshall:	0000-0003-4087-1209
Jason D. Hill:	0000-0001-7609-6713

Abstract

Each year, millions of premature deaths worldwide are caused by exposure to outdoor air pollution, especially fine particulate matter ($PM_{2.5}$). Designing policies to reduce deaths relies on air quality modeling for estimating changes in $PM_{2.5}$ concentrations from many policy scenarios at high spatial resolution. However, air quality modeling typically has high requirements for computation and expertise, which limits policy design, especially in countries where most $PM_{2.5}$-related deaths occur. Lower requirement reduced-complexity models exist but are generally unavailable worldwide. Here, we adapt InMAP, a reduced-complexity model originally developed for the United States, to simulate annual-average primary and secondary $PM_{2.5}$ concentrations across a global-through-urban spatial domain: "Global InMAP". Global InMAP uses a variable resolution grid, with 4 km horizontal grid cell widths in cities. We evaluate Global InMAP performance both against measurements and a state-of-the-science chemical transport model, GEOS-Chem. For the emission scenarios considered, Global InMAP reproduced GEOS-Chem pollutant concentrations with a normalized mean bias of 59%–121%. Global InMAP can be run on a desktop computer; simulations here took 2.6–4.4 hours. This work presents a global, open-source, reduced-complexity air quality model to facilitate air pollution policy assessment worldwide, providing a tool for reducing the deaths where they occur most.

Introduction

Exposure to outdoor air pollution is the largest environmental health risk factor worldwide, associated with millions of excess deaths each year[1,2]. The deaths are mostly attributable to fine particulate matter ($PM_{2.5}$), which can either be emitted directly, or can form indirectly from precursor pollutants that are emitted from a wide variety of natural and anthropogenic emission sources, including transportation, agriculture, and electricity generation[3,4]. Designing strategies to reduce mortality relies on understanding how specific emission sources affect ambient $PM_{2.5}$ concentrations, and thereby, human health, across a range of possible technology or policy scenarios.

InMAP[5] (Intervention Model for Air Pollution) is a reduced-complexity, open-source air quality model that has been used to inform strategies to reduce $PM_{2.5}$-related mortality from specific emission sources. For example, InMAP has been used to estimate fine-scale pollution impacts across distances[6], measures of pollution inequity across racial-ethnic and socioeconomic groups[7], the health impacts of specific sectors under different policy scenarios[8,9], and individual impacts of commodities[10]. However, as with other widely used reduced-complexity air quality models such as EASIUR[11], AP2[12], and COBRA[13], InMAP has only been configured and evaluated for the United States, a country with just 4% of the world's population and around 2% of the world's air quality-related deaths[2,4].

Chemical transport models (CTMs) are employed for estimating the effects of emission sources on pollutant concentrations and health impacts, and are considered state-of-the-science for air quality modeling. However, they require substantial time, expertise, and computational resources (*e.g.*, several computation days per simulation month), limiting the use-cases and therefore the extent to which they can inform many multidimensional policy decisions[5,14], especially when hundreds of policy scenarios are being considered. Although GEOS-Chem is one of the most widely used CTMs, 60% of deaths from outdoor air pollution occur in countries where there are no known users or institutions using GEOS-Chem[15,16].

Some global air quality models are available with a lower operational difficulty than CTMs, including TM5-FASST[17] and source-receptor relationships built from GEOS-Chem adjoint[18] and EMEP[19]. Compared to the existing global air quality models with lower operational difficulty than

CTMs, InMAP has higher spatial resolution, is easier to use, and has lower computational costs. A recent notable effort[20] to build a monthly life cycle assessment model for $PM_{2.5}$ has not yet been tested against measurements or compared with results from a CTM. A diversity of independently evaluated reduced-complexity models will increase their applicability and the robustness of policy assessments worldwide[21].

Here, we developed and configured InMAP for use on a global spatial domain ("Global InMAP"). We ran a year-long, global CTM simulation using GEOS-Chem[22], and used its outputs to globally parameterize the chemistry, physics, and meteorology of InMAP. We then ran InMAP on global emission inventories to predict total $PM_{2.5}$ concentrations as well as changes in concentrations from three specific scenarios of emission changes. We compared the results to a global dataset of ground observations, as well as to $PM_{2.5}$ concentrations and changes in concentrations predicted by GEOS-Chem. Lastly, we compared Global InMAP to the United States versions of InMAP for two emission scenarios.

Materials and Methods

The InMAP modeling framework, fully described in Tessum *et al.*[5], estimates annual-average concentrations of fine particulate matter ($PM_{2.5}$), including both primary (*i.e.*, directly emitted) and secondary (*i.e.*, formed in the atmosphere) components. InMAP explicitly tracks secondary $PM_{2.5}$ contributions from particulate ammonium (pNH_4), particulate sulfate (pSO_4), particulate nitrate (pNO_3), and secondary organic aerosol (SOA), from emissions of $PM_{2.5}$ precursors (sulfur oxides (SO_x), nitrogen oxides (NO_x), ammonia (NH_3), and non-methane volatile organic compounds (NMVOCs)). InMAP estimates pollutant concentrations by approximating the steady-state solution to a set of differential equations governing pollutant emissions, reaction, advection, diffusion, and removal. It solves the equations by discretizing over space and time, using a variable resolution grid, and spatially varying parameterizations that simplify the reaction, advection, and removal terms in the equations. Whereas CTMs simulate chemistry and physics (reaction, advection, removal) using first principles and mechanistic or empirical representations for specific processes, InMAP simulates chemistry and physics using simplified representations that are parameterized by the outputs of a CTM simulation.

InMAP as configured over the United States ("US InMAP") was parameterized using outputs from WRF-Chem[23,24]. However, WRF-Chem is not commonly used for global simulations. Instead, InMAP was parameterized here using outputs from GEOS-Chem[22], a global CTM. Details of the model configuration, GEOS-Chem simulation inputs, global emission inventories, and performance evaluation are provided below.

Global InMAP computational grid

As with previous InMAP configurations for the US[5-10], the horizontal resolution of the Global InMAP computational grid varies across space and is higher in places with larger population or population density. Here, we used 2020 projected population data at 0.01° resolution[25] to create the computational grid. We employed a population density threshold of 5.5×10^8 deg^{-2} and a population threshold of 100,000. For any grid cell, if either threshold was exceeded, then the model subdivided it into smaller cells until the smallest cell size was reached.

The resulting computational grid (Figure S1) has ~1.5 million grid cells (ground-level: 170,358 grid cells), whose horizontal resolution at ground-level ranges from 5° × 4° (which corresponds to ~500 km length at the equator) in remote locations to 0.04° × 0.03° (~4 km length at the equator) in urban locations. The spatial domain encompasses the vast majority of the Earth's surface: latitudes from -87.0° to +81.0° and longitudes from -178.0° to +172.0°. Global InMAP does not

track pollution across the poles or antimeridian[26]. The resulting grid covers all but ~5 million people (< 0.1% of the total population) in parts of New Zealand and other islands in the Pacific Ocean. The population-weighted average grid-cell size is 1,000 km^2 (for comparison, ~39,000 km^2 for GEOS-Chem). The resulting pre-processed gridded input data file is ~700 MB, and is provided in Dataset S1.

GEOS-Chem simulation

Chemical and physical atmospheric parameters used in Global InMAP, such as annual-average gas/particle-phase partitioning coefficients, were derived from the outputs of an annual GEOS-Chem "Classic" (version 11-01f) simulation (2016-01-01 until 2017-01-01), with meteorology provided by MERRA-2[27]. The GEOS-Chem outputs were used in the same way as the corresponding WRF-Chem variables were used for US InMAP (see Tessum *et al.*[5]). The full list of GEOS-Chem variables used in Global InMAP, and descriptions of how they are used, can be found in Table S1.

The GEOS-Chem model code and configuration were derived from a simulation performed by Hammer *et al.*,[28] where the chemical mechanism included complex secondary organic aerosol (SOA) formation with semi-volatile primary organic aerosol[29,30]. We used the standard horizontal spatial resolution for global simulations in GEOS-Chem, 2° × 2.5°, (~ 220 km × 275 km at the equator) with 47 vertical levels, following the configuration described in Hammer *et al.*[28]

GEOS-Chem also allows for higher resolution grids nested within a larger domain[31]. Again following Hammer *et al.*[28], we ran GEOS-Chem nested grid simulations over the same time period for Asia, Europe, and North America, at 0.5° × 0.625° resolution, which covers 75% of the world's population. First, boundary conditions for the nested grid simulations were recorded every 180 minutes of simulation time, at 2° × 2.5° resolution, during the global simulation. In our application, emergent properties extracted for use in Global InMAP, such as the annual-average temperature and wind velocity vectors, are only specified up to this coarse resolution. However, Global InMAP can still be used on a higher resolution (variable) grid, and the resolution of the emission inventory is also not limited by the resolution of the GEOS-Chem output.

Emission inputs

To estimate concentrations of total $PM_{2.5}$ and speciated components using Global InMAP, we compiled a global emission inventory of NH_3, primary $PM_{2.5}$, NO_x, SO_x, and NMVOC. For consistency, we chose the same emission inventories as those used in the GEOS-Chem simulation, but, where possible, processed to a higher spatial resolution as described below for the Global InMAP computational grid. Total annual emissions fluxes for the emission inventories used in the Global InMAP simulation are given in Table 1.

Where possible, the total emission inventories used for the Global InMAP simulation were compiled using the standalone version of HEMCO[32], using the same configuration as used in the GEOS-Chem simulation except at 0.25° × 0.25° horizontal resolution. Differences in grid resolutions, time steps, and environmental fields can result in small differences when the same emission inventories are processed. HEMCO standalone provides both high resolution emissions and consistency with the GEOS-Chem simulation, but cannot be used for some emission inventories that require detailed chemical or meteorological inputs. For those, we instead saved out emissions ("diagnostics") from the GEOS-Chem simulation, gridded at 2° × 2.5°, and used these in the global InMAP simulation. Table 1 gives the total annual emissions for Global InMAP inputs, and the data source for each group of emissions used.

Only a subset of NMVOC emissions is likely to form SOA[33,34]. For Global InMAP anthropogenic emissions, we included isoprene, monoterpenes, benzene, toluene, xylenes, trimethylbenzenes, alkanes with more than 4 carbon atoms, and other aromatics, from the EDGAR[35] v4.3.2 emission inventory. For biogenic emissions, we included limonene, isoprene, alpha-pinene, beta-pinene, sabinene, carene, and monoterpenes from the global GEOS-Chem simulation. For biomass burning, we include benzene, toluene, xylenes, alkenes with more than 3 carbon atoms, and alkanes with more than 4 carbon atoms, from the RETRO biomass burning emission inventory[36].

Although Global InMAP has the functionality to include vertically elevated emissions, there is a lack of global information on emission heights for many sources[35]. HEMCO processed emissions were thus derived at the lowest vertical layer, except for aircraft emissions, lightning NO_x and volcanic SO_x. For simplicity in configuring the Global InMAP emissions, here we only used the emissions from these sources in the lowest vertical layer, which excluded 8% of global NO_x emissions and 16% of global SO_x emissions.

$PM_{2.5}$ concentrations are not directly tracked in GEOS-Chem, but rather are calculated from its underlying components that are grouped in such a way as to facilitate chemical and atmospheric modeling. For example, dust is grouped by several size classes that do not perfectly map onto $PM_{2.5}$. HEMCO and GEOS-Chem diagnostic outputs also typically report emissions in these groups, requiring some conversions for use in Global InMAP. Here, we did so in accordance with the standard GEOS-Chem recommendations (see Table S1 for the $PM_{2.5}$ equation used). Following Hammer *et al.*[28] and Li *et al.*[37], irreversible aqueous formation of SOA from isoprene was included in total $PM_{2.5}$ mass, whereas reversible formation was excluded.

InMAP data inputs for pollutant removal through deposition likewise required modification for Global InMAP simulations. Specifically, Global InMAP requires land cover data to calculate dry deposition rates for gases and particles in each ground-level grid cell. For the United States, InMAP used land cover data from the United States Geological Survey National Land Cover Database[38]. For Global InMAP, we instead used the Olson 2001 Land Use Map at 0.025° × 0.025° resolution[39], which is also used in GEOS-Chem.

Comparison with other air quality models and measurements

Using the global emission inventories described in the previous section, we generated Global InMAP results and compared them against other models and measurements (1) for total concentrations; (2) for three perturbation scenarios wherein we modified global emissions from a specific sector and predicted the resulting concentration changes; and (3) for United States electricity and transportation emissions, to compare Global InMAP with US InMAP.

First, we evaluated Global InMAP predictions of $PM_{2.5}$ (total and speciated) against annual-average ground-level measurements, as is commonly done for air quality models[40,41]. To this end, we compiled and vetted a global measurement dataset for total and speciated $PM_{2.5}$ (see Supplementary Text and Table S2 for additional details). We reported metrics commonly used for evaluating model performance: normalized mean error and bias (NME and NMB), the squared linear correlation coefficient, R^2, and the slope of the best-fit line, S (see Supplementary Information for equations used)[42]. Using this approach, model-measurement comparisons were generated for Global InMAP and (separately) for the GEOS-Chem simulation (described above).

To provide context for the model-measurement comparison results, we reported model criteria published by Emery *et al.*[42] (see Supplementary Information). Performance criteria were provided as a general reference point, not as “pass/fail” criteria. The criteria are intended for evaluating $PM_{2.5}$ concentrations over sub-annual lengths of time[43], or for daily average measurements within

1000 km, where there are more than 10 measurements[42]. Here, we used the criteria more broadly to identify the stronger and weaker aspects of model performance.

Second, we simulated the effects of three emissions perturbations with Global InMAP and GEOS-Chem simulations and compared their predicted pollutant concentration increments. The perturbations chosen were: (i) a 100% increase (4.9 Tg) in global SO_2 emissions from power generation for 2 months (2016-01-01 until 2016-03-01); (ii) a 100% increase (7.5 Tg) in global NH_3 emissions from agricultural soils for 3 months (2016-01-01 until 2016-04-01); (iii) a 100% increase (1.4 Tg) in global NO_x emissions from road transport for 1 month (2016-01-01 until 2016-02-01). All emissions changes were from the EDGAR emissions database (v.4.2, 0.1° × 0.1° resolution) as described above. For each of the scenarios chosen, we ran global, annual 2° × 2.5° GEOS-Chem simulations similar to those described above, with the change in emissions implemented using a constant temporal profile over the timescale of the perturbation. As InMAP is an "intervention" model (designed to model changes in emissions directly), for Global InMAP we ran the changes in emissions from the EDGAR emission inventories at native resolution.

Lastly, because InMAP has already been configured and evaluated over the contiguous United States, we performed two simulations for United States emission changes using Global InMAP and US InMAP. To this end, we compiled emission inventories over the United States using the National Emissions Inventory (NEI) 2014v.1, processed exactly as in Thakrar *et al.*[8] We investigated two sources of $PM_{2.5}$ and precursor emissions: coal-powered electricity generation (NEI Source Classification Code: 10100212) and gasoline passenger vehicles (NEI Source Classification Code: 2201210080).

Results

Computational requirements

The annual, global simulations described above (system: 98 processors on 1 node of a supercomputing cluster; 36 GB memory) required 4 hours for Global InMAP (1.5 million grid cells) and 100 hours for GEOS-Chem (2° × 2.5° grid resolution, 0.6 million grid cells). The perturbation simulations, when run on the same system, took 2.6–4.4 hours.

Other GEOS-Chem simulations require comparably high resources[44]. The variable resolution InMAP grid allows for much higher spatial resolution over areas with high population density than is possible with the GEOS-Chem uniform grid, while only requiring 4% of the computational time.

Model-to-measurement comparisons

The Global InMAP simulation using total emissions was able to predict total $PM_{2.5}$ concentrations against measurements globally with NMB = –60%; NME = 63%; and R^2 = 0.35 (see Figures 1–2, S2). As with the GEOS-Chem simulation, the performance of the Global InMAP simulation varied by region (see Figures S3–S8). The Global InMAP simulation was generally most accurate in Oceana (NMB: -45%; R^2: 0.64; see Figure S7), North America (NMB: -54%; R^2: 0.59; see Figure S6), and Europe (NMB: -64%; R^2: 0.28; see Figure S5), and least accurate in South America (NMB: -74%; R^2: 0.05; see Figure S8). Across many heavily polluted regions in Asia, the Global InMAP simulation predicted much lower $PM_{2.5}$ concentrations than are measured (difference: > 30 μg m^{-3}) (Figure S4), in particular across the Indo-Gangetic Plain. The underprediction may have arisen because of potentially low emissions inputs, *e.g.* from industrial and agricultural NH_3 emissions[45] or missing NMVOC species from biomass burning[46]. The Global InMAP simulation may have underpredicted pollution from episodic events, such as biomass burning in the Indo-Gangetic Plain, because Global InMAP assumes that emissions occur at an annual-average rate.

Furthermore, the chemistry that is included in Global InMAP may not be sufficiently complex to accurately predict $PM_{2.5}$ in heavily polluted areas[47].

We also compared annual-average predicted concentrations from the Global InMAP simulation to annual-average measurements of pSO_4, pNO_3, and pNH_4 globally (Figures 3–4). The Global InMAP simulation predicted these components reasonably well (NME: 50%–67%; R^2: 0.24–0.38) and was generally biased low against measurements for pNO_3 (especially in areas with pNO_3 >2 $\mu g\ m^{-3}$), and high for pSO_4 and pNH_4. Because the Global InMAP simulation did not have a strong low bias against secondary inorganic $PM_{2.5}$ measurements, it is likely that much of the low bias of the Global InMAP simulation against total $PM_{2.5}$ measurements arose from its prediction of primary $PM_{2.5}$ concentrations (see Figure 3). However, measurement data for SOA and primary $PM_{2.5}$ concentrations were not available at the evaluation sites (see Figure 3 for ground-level concentrations of these species).

We also compared the GEOS-Chem simulation against the same measurement data, to contextualize the Global InMAP results. The GEOS-Chem simulation predicted total $PM_{2.5}$ measurements with an R^2 of 0.55. For comparison, a GEOS-Chem simulation that used the same code and emissions[28] reported an R^2 of 0.61 when using a more comprehensive measurement dataset and averaging results across years 2010–2018 instead of just 2016.

Both the Global InMAP and the GEOS-Chem simulations predicted lower annual-average total $PM_{2.5}$ concentrations than were observed. For all species and regions, the direction of bias against measurements was the same for the Global InMAP simulation as for the GEOS-Chem simulation. This suggests that the Global InMAP simulation was inheriting the bias from the GEOS-Chem simulation inputs to some extent. If that was the case, then future improvements to the GEOS-Chem model and to the emission inventories used here could further reduce Global InMAP biases.

The Global InMAP simulation broadly reproduced spatial patterns of pollutant concentrations predicted by GEOS-Chem. However, there were some features present in the GEOS-Chem simulation that were not captured by the Global InMAP simulation. Such features included high annual-average $PM_{2.5}$ concentrations from biomass burning, including the Alberta fires, crop burning in the Indo-Gangetic Plain, peatland fires in Singapore and Malaysia, and burning in Siberia. InMAP may have underpredicted $PM_{2.5}$ concentrations from biomass burning relative to the GEOS-Chem simulation because it assumes emissions happen at an annual-average rate. Across Western China, the Global InMAP simulation tended to misrepresent the spatial patterns provided by the parent GEOS-Chem simulation for both primary and secondary $PM_{2.5}$, including high concentrations over the Himalayas and Sichuan Basin, and low concentrations in surrounding areas. This may suggest that the annual-average advection scheme used by InMAP does not yet adequately capture complex air flows over steep terrain.

Evaluation of predicted responses to changes in emissions

The major intended use of InMAP is to estimate the changes in human exposure to $PM_{2.5}$ concentrations for given scenarios of emission changes. Therefore, its ability to reproduce the changes predicted by the original CTM could be considered its most important attribute and is more important than its ability to reproduce current absolute concentrations. However, InMAP is designed to predict human exposure with high spatial resolution in urban areas, while GEOS-Chem is designed to predict global chemical transport and runs at comparatively low resolution. Directly comparing the two models requires re-gridding the higher-resolution Global InMAP results to match the lower-resolution GEOS-Chem results, which cancels out predictive advantages Global InMAP might gain from its use of higher spatial resolution. Therefore, results

in this section could be considered a conservative evaluation of Global InMAP's predictive performance.

Figure 5 shows annual-average pollutant concentration increments predicted by the GEOS-Chem and Global InMAP simulations for increases in SO_x emissions from power generation, NH_3 emissions from agricultural soils, and NO_x emissions from road transportation. When regridding Global InMAP predictions to the GEOS-Chem grid, we found that Global InMAP reproduced the GEOS-Chem results with an average area-weighted NME of 118–182% and an average area-weighted NMB of 59–121% (see Table 2). For the NO_x and NH_3 emissions scenarios, Global InMAP exhibited better performance against GEOS-Chem on a population-weighted basis than on an area-weighted basis. For the SO_x emissions scenario, Global InMAP exhibited the lowest performance against the GEOS-Chem simulation, having overpredicted changes in pSO_4 concentrations especially in populated areas.

The Global InMAP simulations predicted greater variability in concentration changes over urban areas than the 2° × 2.5° GEOS-Chem simulations for the same emissions scenarios, owing to its higher resolution computational grid. Figure 6 compares the pNO_3 concentration changes over Cairo, São Paulo, and Tokyo (the largest cities in Africa, South America, and Asia[48]) for the NO_x perturbation scenario as predicted by Global InMAP and GEOS-Chem. Changes in concentrations predicted by Global InMAP correlated with changes in emissions at the urban scale. Higher resolution GEOS-Chem simulations that resolve intra-urban gradients would be even more computationally expensive than the GEOS-Chem simulations performed here[44].

Global InMAP predicted similar spatial patterns and magnitudes of changes in pollutant concentrations as did US InMAP for a given emissions perturbation (see Figure S7), with NME and NMB within ± 50% for both scenarios considered (see Table 2). This demonstrated consistency between the InMAP versions derived from WRF-Chem and GEOS-Chem inputs, suggesting that no major errors were introduced in the Global InMAP model development (see Table S1; Tessum *et al.*[5]). For InMAP applications focusing only on the United States, continued use of US InMAP is warranted, as the WRF-Chem simulation used to parameterize US InMAP provides higher spatial resolution than does the nested GEOS-Chem simulation employed for Global InMAP.

Discussion

Here, we extended InMAP, a reduced-complexity air quality model originally developed for use in the United States, to simulate a global-through-urban spatial domain. InMAP is designed to supplement rather than supplant tools like GEOS-Chem or other global models, *e.g.*, for cases in which resources to implement a CTM are unavailable, or when hundreds of simulations are needed to evaluate a large variety of policy scenarios and perform an initial assessment and screening.

Global InMAP requires relatively low computational resources, allowing it to be run on a desktop computer rather than a super-computer. Simulations predicting annual-average concentrations take several hours rather than days. For example, compared to the global GEOS-Chem simulation described here, the Global InMAP simulation was 25× faster at predicting total annual-average $PM_{2.5}$ concentrations, despite having 39× higher population-weighted average spatial resolution (down to ~4km in urban areas).

As expected, the expedience of Global InMAP comes at the expense of lower predictive accuracy compared to a comprehensive CTM. This Global InMAP simulation is biased low against measurements for total $PM_{2.5}$ across all regions. Among species, it is biased high against

393 measurements of pSO_4 and pNH_4, and low against measurements of pNO_3. The low
394 computational resource requirements make Global InMAP particularly well-suited to applications
395 where hundreds of policy scenarios are evaluated, as is often done using reduced-complexity
396 models for the United States[8,10,49], or when no other air quality models are available at the urban
397 scale. In places with higher population and pollution exposure than the United States, there is
398 even more potential for a reduced-complexity model such as Global InMAP to inform impactful
399 policy decisions. Global InMAP may be important for informing preliminary hypotheses about
400 policy decisions in its early stages (*e.g.*, "What is the best location to site a new facility that may
401 be a major pollution source?"), allowing computational resources to be used instead for CTMs at
402 a later stage to check consistency with the findings.
403
404 Global InMAP performance varies regionally, and it tends to perform worse against
405 measurements in places where GEOS-Chem also performs poorly (*e.g.*, South America). This
406 suggests that predictive accuracy in those areas is generally lower across models, so that Global
407 InMAP may provide a comparative advantage. Further, this suggests that Global InMAP
408 performance in those regions may improve based on future advancements in emission
409 inventories or GEOS-Chem model inputs.
410
411 By directly estimating annual-average $PM_{2.5}$ concentrations at high spatial resolution, Global
412 InMAP is configured to easily estimate changes in human exposure and health impacts. When
413 estimating human health effects of emissions changes, there will also be sizeable uncertainties
414 from estimating the emissions changes themselves and from the concentration-response function
415 employed[50]; Global InMAP errors should thus be contextualized with those in mind. For the
416 United States, a previous study[6] found that the largest source of uncertainty in estimating
417 monetized $PM_{2.5}$ health impacts was the economic valuation of premature mortality, followed by
418 the concentration response function, whereas uncertainty in $PM_{2.5}$ concentrations from the choice
419 of air quality model was the smallest source of uncertainty considered.
420
421 Here, by providing a global, open source, air quality model with high spatial resolution and low
422 computational requirements, we hope to facilitate the wide practice of air pollution policy
423 assessment worldwide.

Acknowledgments

The authors thank Peter Adams, Susan Anenberg, Zoe Chafe, Xin Chen, Kimberly Colgan, Nina Domingo, Madisen Gittlin, Melanie Hammer, Daven Henze, Iyad Kheirbek, Gary Kleiman, Chi Li, Randall Martin, Dev Millstein, Shayak Sengupta, Kelley Wells, Ruili Wu, and Xueying Yu.

This project was funded by the US EPA (Assistance Agreement No. R835873 to CACES; J.S.A., S.B., J.D.H, J.D.M, D.B.M., S.N.P., C.W.T, S.K.T.), the Clean Air Fund via c40 (J.D.M., C.W.T.), the Wellcome Trust (Grant 216075/Z/19/Z; J.D.M., C.W.T.), the William F. Wilcke Fellowship Fund (S.K.T.), and USDA/NIFA (Project MIN-12-110; J.D.H.). The manuscript has not been formally reviewed by the funders; the views expressed in this document are solely those of authors and do not necessarily reflect those of the funders. Funders do not endorse any products or commercial services mentioned in this publication, and no endorsement of the funders or their goals or affiliates is implied.

The authors declare no competing financial interest.

References

1. Landrigan, P. J.; Fuller, R.; Acosta, J. R.; Adeyi, O.; Arnold, R.; Basu, N.; Baldé, A. B.; Bertollini, R.; Bose-O'Reilly, S.; Boufford, J. I., et al. The Lancet Commission on pollution and health. *Lancet* **2018**, *391* (10119), 462-512.
2. Burnett, R.; Chen, H.; Szyszkowicz, M.; Fann, N.; Hubbell, B.; Pope III, C. A.; Apte, J. S.; Brauer, M.; Cohen, A.; Weichenthal, S., et al. Global estimates of mortality associated with long-term exposure to outdoor fine particulate matter. *Proc. Natl. Acad. Sci. U.S.A.* **2018**, *115* (38), 9592-9597.
3. Silva, R. A.; Adelman, Z.; Fry, M. M.; West, J. J. The impact of individual anthropogenic emissions sectors on the global burden of human mortality due to ambient air pollution. Environ. Health Perspect. **2016**, *124* (11), 1776-1784.
4. Lelieveld, J.; Evans, J. S.; Fnais, M.; Giannadaki, D.; Pozzer, A. The contribution of outdoor air pollution sources to premature mortality on a global scale. *Nature* **2015**, *525* (7569), 367.
5. Tessum, C. W.; Hill, J. D.; Marshall, J. D. InMAP: A model for air pollution interventions. *PLoS ONE* **2017,** *12* (4), e0176131.
6. Goodkind, A. L.; Tessum, C. W.; Coggins, J. S.; Hill, J. D.; Marshall, J. D. Fine-scale damage estimates of particulate matter air pollution reveal opportunities for location-specific mitigation of emissions. *Proc. Natl. Acad. Sci. U.S.A.* **2019,** *116* (18), 8775-8780.
7. Tessum, C. W.; Apte, J. S.; Goodkind, A. L.; Muller, N. Z.; Mullins, K. A.; Paolella, D. A.; Polasky, S.; Springer, N. P.; Thakrar, S. K.; Marshall, J. D., et al. Inequity in consumption of goods and services adds to racial–ethnic disparities in air pollution exposure. *Proc. Natl. Acad. Sci. U.S.A.* **2019,** *116* (13), 6001-6006.
8. Thakrar, S.K.; Balasubramanian, S.; Adams, P.J.; Azevedo, I.M.; Muller, N.Z.; Pandis, S.N.; Polasky, S.; Pope III, C.A.; Robinson, A.L.; Apte, J.S., et al. Reducing mortality from air pollution in the United States by targeting specific emission sources. *Environ. Sci. Technol. Lett.* **2020**, *7* (9), pp.639-645.
9. Liu, L.; Hwang, T.; Lee, S.; Ouyang, Y.; Lee, B.; Smith, S. J.; Tessum, C. W.; Marshall, J. D.; Yan, F.; Daenzer, K., et al. Health and climate impacts of future United States land freight modelled with global-to-urban models. Nature Sustainability **2019**, 2(2), 105-112.
10. Hill, J., Goodkind, A.; Tessum, C.; Thakrar, S.; Tilman, D.; Polasky, S.; Smith, T.; Hunt, N.; Mullins, K.; Clark, M., et al. Air quality-related health damages of maize. *Nat. Sustain.* **2019**, *2* (5), 397-403.

11. Heo, J.; Adams, P. J.; Gao, H. Reduced-form modeling of public health impacts of inorganic $PM_{2.5}$ and precursor emissions. *Atmos. Environ.* **2016,** *137,* 80-89.
12. Muller, N. Z. Boosting GDP growth by accounting for the environment. *Science* **2014,** *345* (6199), 873-74.
13. USEPA. User's manual for the co-benefits risk assessment (COBRA), 2018.
14. Lee, C. J.; Martin, R. V.; Henze, D. K.; Brauer, M.; Cohen, A.; van Donkelaar, A. Response of global particulate-matter-related mortality to changes in local precursor emissions. *Environ. Sci. Technol.* **2015**, *49* (7), 4335-4344.
15. GBD Results Tool. Accessed: 25th January 2021. http://ghdx.healthdata.org/gbd-results-tool
16. Maps of GEOS-Chem User Groups. Accessed: 25th January 2021. http://acmg.seas.harvard.edu/geos/geos_people.html
17. Van Dingenen, R.; Dentener, F.; Crippa, M.; Leitao, J.; Marmer, E.; Rao-Skirbekk, S.; Solazzo, E.; Valentini, L. TM5-FASST: A global atmospheric source-receptor model for rapid impact analysis of emission changes on air quality and short-lived climate pollutants. *Atmos. Chem. Phys.* **2018**, *18*, 16173-16211.
18. Henze, D. K.; Hakami, A.; Seinfeld, J. H. Development of the adjoint of GEOS-Chem. *Atmos. Chem. Phys.* **2007**, *7* (9), 2413-2433.
19. Amann, M.; Bertok, I.; Borken-Kleefeld, J.; Cofala, J.; Heyes, C.; Höglund-Isaksson, L.; Klimont, Z.; Nguyen, B.; Posch, M.; Rafaj, P.; Sandler, R.; *et al.* Cost-effective control of air quality and greenhouse gases in Europe: Modeling and policy applications. *Environ. Model. Softw.* **2011**, *26* (12), 1489-1501.
20. Oberschelp, C.; Pfister, S.; Hellweg, S. Globally regionalized monthly life cycle impact assessment of particulate matter. *Environ. Sci. Technol.* **2020**, *54* (24), 16028-16038.
21. Gilmore, E. A.; Heo, J.; Muller, N. Z.; Tessum, C. W.; Hill, J. D.; Marshall, J. D.; Adams, P. J. An inter-comparison of air quality social cost estimates from reduced-complexity models. *Environ. Res. Lett.* **2019,** *14* (7), 074016.
22. Bey, I.; Jacob, D. J.; Yantosca, R. M.; Logan, J. A.; Field, B. D.; Fiore, A. M.; Li, Q.; Liu, H. Y.; Mickley, L. J.; Schultz, M. G. Global modeling of tropospheric chemistry with assimilated meteorology: Model description and evaluation. *J. Geophysi. Res. Atmos.* **2001**, *106* (D19), 23073-23095.
23. Grell, G. A.; Peckham, S. E.; Schmitz, R.; McKeen, S. A.; Frost, G.; Skamarock, W. C.; Eder, B. Fully coupled online chemistry within the WRF model. Atmos. Environ. **2005**, 39(37), 6957-6975.
24. Tessum, C. W.; Hill, J. D.; Marshall, J. D. Twelve-month, 12km resolution north american WRF-Chem v3. 4 air quality simulation: performance evaluation. *Geosci. Mod. Dev.* **2015**, *8* (4).
25. Gridded Population of the World, Version 4 (GPWv4): National Identifier Grid. Palisades, NY: NASA Socioeconomic Data and Applications Center (SEDAC). http://dx.doi.org/10.7927/H41V5BX1.
26. Park, R. J.; Jacob, D. J.; Field, B. D.; Yantosca, R. M.; Chin, M. Natural and transboundary pollution influences on sulfate-nitrate-ammonium aerosols in the United States: Implications for policy. *J. Geophys. Res. Atmos.* **2004**, *109* (D15).
27. Gelaro, R.; McCarty, W.; Suárez, M. J.; Todling, R.; Molod, A.; Takacs, L.; Randles, C. A.; Darmenov, A.; Bosilovich, M. G.; Reichle, R., *et al.* The modern-era retrospective analysis for research and applications, version 2 (MERRA-2). *J. Clim.* **2017**, *30* (14), 5419-5454.
28. Hammer, M.S.; van Donkelaar, A.; Li, C.; Lyapustin, A.; Sayer, A.M.; Hsu, N.C.; Levy, R.C.; Garay, M.J.; Kalashnikova, O.V.; Kahn, R.A.; Brauer, M. Global estimates and long-term trends of fine particulate matter concentrations (1998–2018). *Environ. Sci. Technol.* **2020**, *54* (13), 7879-7890.

29. Pye, H. O. T; Seinfeld, J. H. A global perspective on aerosol from low-volatility organic compounds. Atmospheric Chemistry and Physics **2010**, *10* (9), 4377-4401.
30. Pye, H. O. T.; Chan, A. W. H.; Barkley, M. P.; Seinfeld, J. H. Global modeling of organic aerosol: the importance of reactive nitrogen (NOx and NO3). Atmospheric Chemistry and Physics **2010**, *10* (22), 11261-11276.
31. Wang, Y. X.; McElroy, M. B.; Jacob, D. J.; Yantosca, R. M. A nested grid formulation for chemical transport over asia: Applications to CO. *J. Geophys. Res. Atmos.* **2004**, *109* (D22).
32. Keller, C. A.; Long, M. S.; Yantosca, R. M.; Da Silva, A. M.; Pawson, S.; Jacob. D. J.; HEMCO v1. 0: A versatile, ESMF-compliant component for calculating emissions in atmospheric models. *Geosci. Model Dev.* **2014**, *7* (4), 1409–1417.
33. Ahmadov, R.; McKeen, S. A.; Robinson, A. L.; Bahreini, R.; Middlebrook, A. M.; De Gouw, J. A.; Meagher, J.; Hsie, E. Y.; Edgerton, E.; Shaw, S., et al. A volatility basis set model for summertime secondary organic aerosols over the eastern united states in 2006. *J Geophys. Res. Atmos.* **2012**, *117* (D6).
34. Philip, S.; Martin, R. V.; Pierce, J. R.; Jimenez, J. L.; Zhang, Q.; Canagaratna, M. R.; Spracklen, D. V.; Nowlan, C. R.; Lamsal, L. N.; Cooper, M. J., et al. Spatially and seasonally resolved estimate of the ratio of organic mass to organic carbon. *Atmos. Environ.* **2014**, *87*, 34-40.
35. Crippa, M.; Guizzardi, D.; Muntean, M.; Schaaf, E.; Dentener, F.; van Aardenne, J. A.; Monni, S.; Doering, U.; Olivier, J. G. J.; Pagliari, V., et al. Gridded emissions of air pollutants for the period 1970-2012 within edgar v4. 3.2. *Earth Syst. Sci. Data* **2018**, *10* (4), 1987-2013.
36. Schultz, M. G.; Heil, A.; Hoelzemann, J. J.; Spessa, A.; Thonicke, K.; Goldammer, J.; Held, A. C.; Pereira, J. M.; van het Bolscher, M. Global Wildland Fire Emissions from 1960 to 2000, *Global Biogeochem. Cyc.* **2008**, *22* (2), GB2002.
37. Li, C.; Martin, R. V.; van Donkelaar, A.; Boys, B. L.; Hammer, M. S.; Xu, J. W.; Marais, E. A.; Reff, A.; Strum, M.; Ridley, D. A., *et al.* Trends in chemical composition of global and regional population-weighted fine particulate matter estimated for 25 years. Environmental science & technology **2017**, *51* (19), 11185-11195.
38. Homer, C.; Huang, C.; Yang, L.; Wylie, B.; Coan, M. Development of a 2001 national land-cover database for the United States. Photogrammetric Engineering & Remote Sensing **2004**, *70* (7), 829-840.
39. GEOS-Chem Wiki. Olson land map. Accessed: 25th January 2021. http://wiki.seas.harvard.edu/geos-chem/index.php/Olson_land_map
40. Dennis, R.; Fox, T.; Fuentes, M.; Gilliland, A.; Hanna, S.; Hogrefe, C.; Irwin, J.; Rao, S. T.; Scheffe, R.; Schere, K., et al. A framework for evaluating regional-scale numerical photochemical modeling systems. *Environ. Fluid Mech.* **2010**, 10(4), 471-489.
41. Diao, M.; Holloway, T.; Choi, S.; O'Neill, S. M.; Al-Hamdan, M. Z.; Van Donkelaar, A.; Martin, R. V.; Jin, X.; Fiore, A. M.; Henze, D. K., et al. Methods, availability, and applications of pm2. 5 exposure estimates derived from ground measurements, satellite, and atmospheric models. *J. Air Waste Manag. Assoc.* **2019**, *69* (12),1391-1414.
42. Emery, C.; Liu, Z.; Russell, A. G.; Odman, M. T.; Yarwood, G.; Kumar, N. Recommendations on statistics and benchmarks to assess photochemical model performance. *J. Air Waste Manag. Assoc.* **2017**, *67* (5), 582-598.
43. Boylan, J. W.; Russell, A. G. PM and light extinction model performance metrics, goals, and criteria for three-dimensional air quality models. *Atmos. Environ.* **2006**, 40(26), 4946-4959.
44. Eastham, S. D.; Long, M. S.; Keller, C. A.; Lundgren, E.; Yantosca, R. M.; Zhuang, J.; Li, C.; Lee, C. J.; Yannetti, M.; Auer, B. M., et al. GEOS-Chem High Performance (GCHP): A next-generation implementation of the GEOS-Chem chemical transport model for massively parallel applications, *Geosci. Model Dev. Discuss.* **2018**, 1-18.

45. Van Damme, M; Clarisse, L.; Whitburn, S.; Hadji-Lazaro, J.; Hurtmans, D.; Clerbaux, C.; Coheur, P-F. Industrial and agricultural ammonia point sources exposed. *Nature* **2018**, *564* (7734), 99-103.
46. Akherati, A.; He, Y.; Coggon, M. M.; Koss, A. R.; Hodshire, A. L.; Sekimoto, K.; Warneke, C.; de Gouw, J.; Yee, L.; Seinfeld, J. H.; Onasch, T.B. Oxygenated aromatic compounds are important precursors of secondary organic aerosol in biomass-burning emissions. Environmental Science & Technology **2020**, *54* (14), 8568-8579.
47. Zheng, B.; Zhang, Q.; Zhang, Y.; He, K. B.; Wang, K.; Zheng, G. J.; Duan, F. K.; Ma, Y. L.; Kimoto, T. Heterogeneous chemistry: a mechanism missing in current models to explain secondary inorganic aerosol formation during the January 2013 haze episode in North China. *Atmos. Chem. Phys.* **2015**, *15*, 2031–2049.
48. United Nations, Department of Economic and Social Affairs, Population Division (2019). World Urbanization Prospects: The 2018 Revision (ST/ESA/SER.A/420). New York: United Nations.
49. Muller, N. Z.; Mendelsohn, R. Efficient pollution regulation: getting the prices right. *Am. Econ. Rev.* **2009**, *99* (5), 1714-39.
50. Coffman, E.; Burnett, R.T.; Sacks, J.D. Quantitative characterization of uncertainty in the concentration–response relationship between long-term $PM_{2.5}$ exposure and mortality at low concentrations. *Environ. Sci. Technol.* **2020**, *54* (16), 10191-10200.

Figures and Tables

Table 1. $PM_{2.5}$ and precursor emissions inputs into GEOS-Chem and Global InMAP.

Pollutant	GEOS-Chem (Tg/yr)	Global InMAP (Tg/yr)	Global InMAP data source	Maximum resolution
Anthropogenic				
$PM_{2.5}$	24.45	32.93	HEMCO	0.25° × 0.25°
NH_3	51.52	47.39	HEMCO	0.25° × 0.25°
SO_x	84.33	84.33	Diagnostics	2° × 2.5°
NO_x	64.85	76.28	HEMCO	0.25° × 0.25°
NMVOC	- [b]	58.15	EDGAR	0.1° × 0.1°
Natural				
$PM_{2.5}$	244.53	244.53	Diagnostics	2° × 2.5°
NH_3	17.38	15.97	HEMCO	0.25° × 0.25°
SO_x	28.32	0.42[a]	Diagnostics	2° × 2.5°
NO_x	28.02	16.60[a]	Diagnostics	2° × 2.5°
NMVOC	- [b]	553.14	Diagnostics	2° × 2.5°
Biomass burning				
$PM_{2.5}$	35.30	35.30	GFED-4	0.25° × 0.25°
NH_3	4.24	4.24	GFED-4	0.25° × 0.25°
SO_x	2.25	2.25	GFED-4	0.25° × 0.25°
NO_x	20.28	20.28	GFED-4	0.25° × 0.25°
NMVOC	- [b]	5.10	RETRO	0.5° × 0.5°

[a]Only NO_x and SO_x emissions in the lowest vertical layer were used in Global InMAP, yet the majority of natural NO_x and SO_x emissions are emitted from lightning and volcanoes at higher levels. [b]Not all NMVOC emissions from GEOS-Chem simulation are reported.

Table 2. Area- and population-weighted normalized mean bias (NMB) and error (NME) for Global InMAP predicted changes in concentrations against changes in concentrations from GEOS-Chem or US InMAP, arising from scenarios of changes in emissions. Positive bias indicates that Global InMAP has higher average concentration changes than the other model.

Model comparison	Scenario	Weighting	NME (%)	NMB (%)
Global InMAP against GEOS-Chem	NH_3 increase from agricultural soils	area-wtd.	118.2	58.7
		population-wtd.	88.6	52.5
	NO_x increase from road transportation	area-wtd.	180.7	96.2
		population-wtd.	102.2	40.8
	SO_x increase from power generation	area-wtd.	181.3	120.7
		population-wtd.	273.4	259.3
Global InMAP against US InMAP	Coal-powered electricity	area-wtd.	38.4	-18.8
		population-wtd.	38.7	-10.5
	Gasoline passenger vehicles	area-wtd.	48.4	-23.0
		population-wtd.	48.8	-46.7

Figure 1. Annual-average ground-level total $PM_{2.5}$ concentrations from the Global InMAP and GEOS-Chem simulations for year 2016.

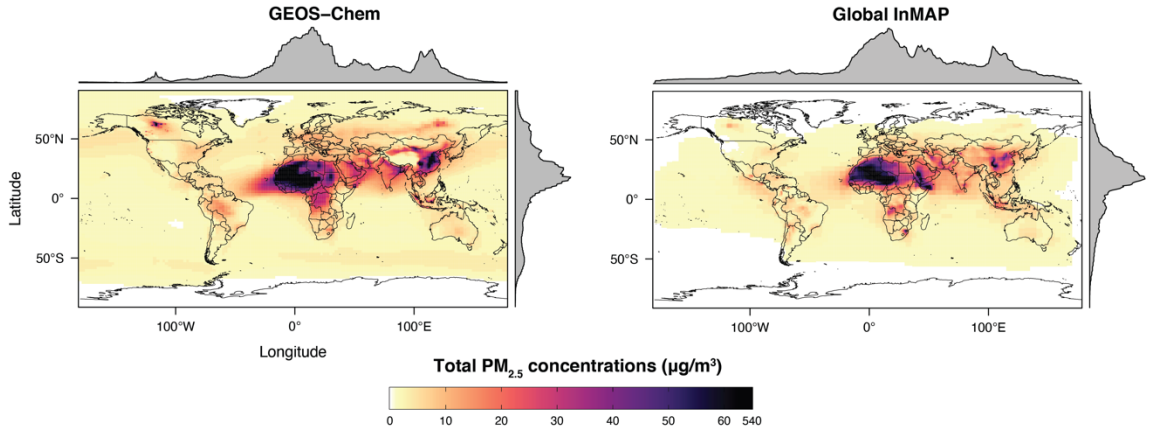

Figure 2. Annual-average total $PM_{2.5}$ concentrations from the Global InMAP and GEOS-Chem simulations against measurements. Only values ≤100 μg m^{-3} are plotted here, excluding 25 (1.5%) model-measurement pairs (full figure shown in Supplementary Information, Figure S2).

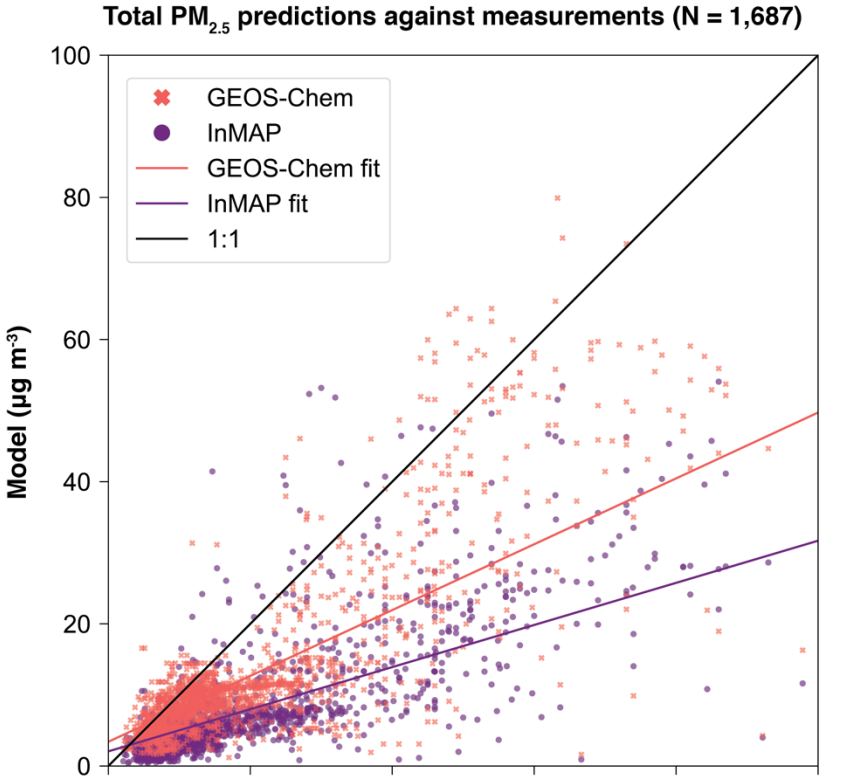

	NMB	NME	Slope	R^2
GEOS-Chem	-37%	41%	0.46	0.55
Global InMAP	-60%	63%	0.30	0.35

Figure 3. Global InMAP and GEOS-Chem annual-average ground-level pNH_4, pNO_3, pSO_4, SOA, and primary $PM_{2.5}$ concentrations.

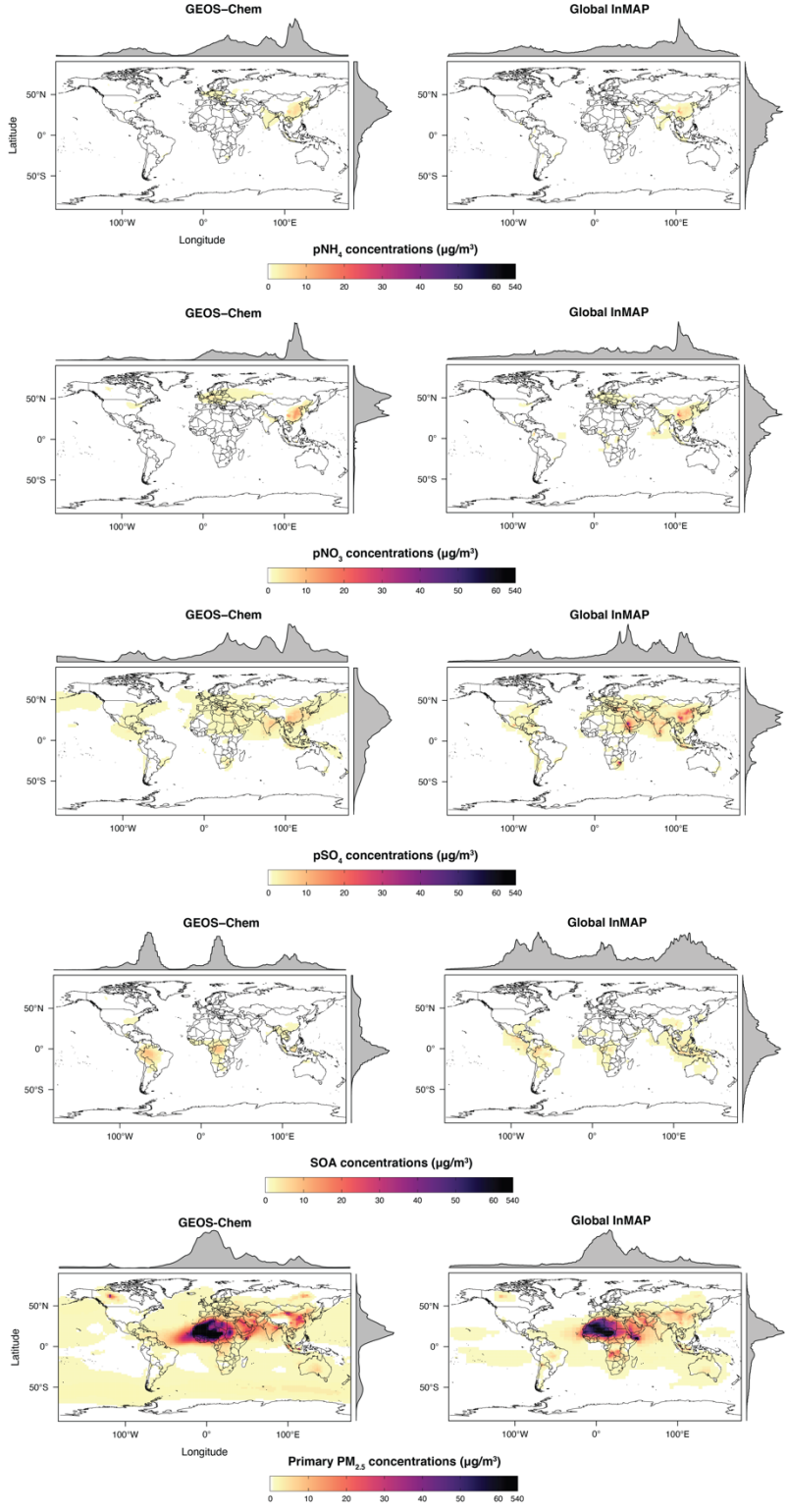

Figure 4. Global InMAP and GEOS-Chem annual-average pSO_4, pNO_3, and pNH_4 concentrations against measurements.

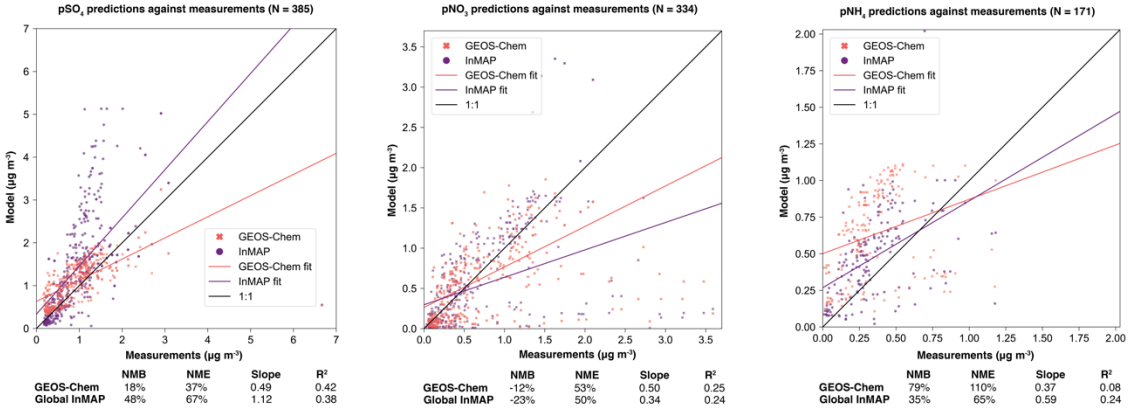

Figure 5. Comparison between Global InMAP and GEOS-Chem for predicting changes in pollutant concentrations. Column (c) shows the difference in concentrations between Global InMAP and GEOS-Chem. *First row:* changes in pSO_4 concentrations from a 100% increase in SO_x emissions from power generation. *Second row:* changes in pNH_4 concentrations from a 100% increase in NH_3 emissions from agricultural soils. *Third row:* changes in pNO_3 concentrations from a 100% increase in NO_x emissions from road transportation.

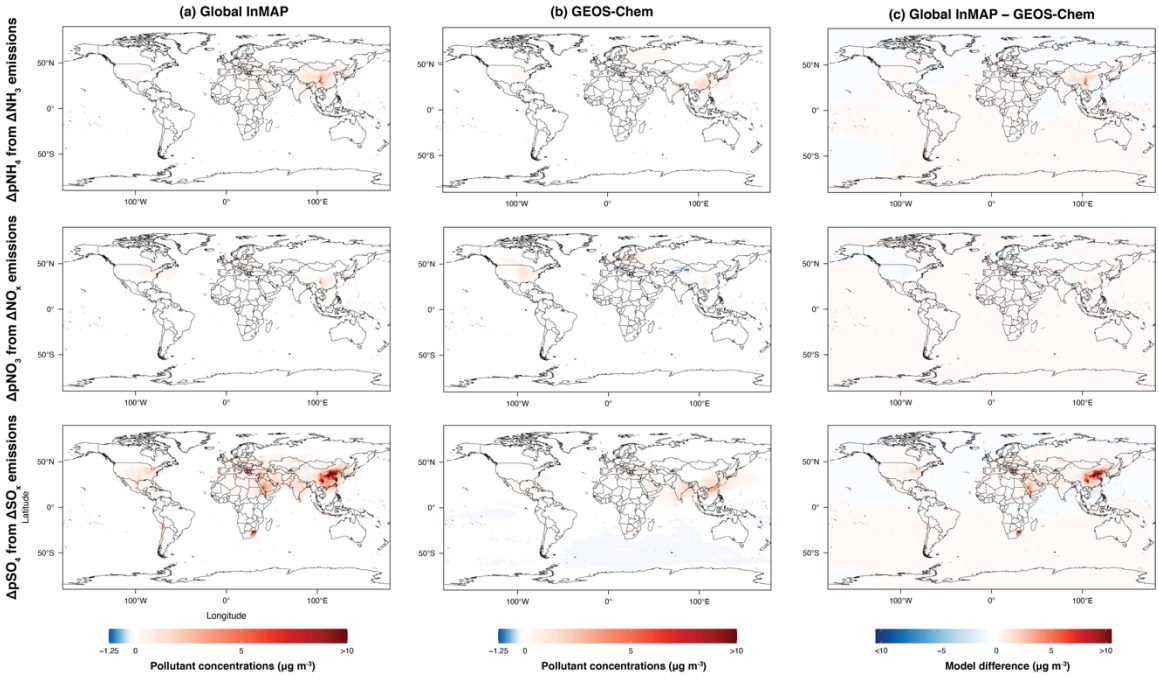

Figure 6. *First column:* 100% increase in NO_x emissions from road transport across Cairo, São Paulo, and Tokyo. *Second and third column:* resulting changes in pNO_3 concentrations predicted by the Global InMAP and the GEOS-Chem simulations. For each map, blue lines indicate rivers and black lines indicate land borders.

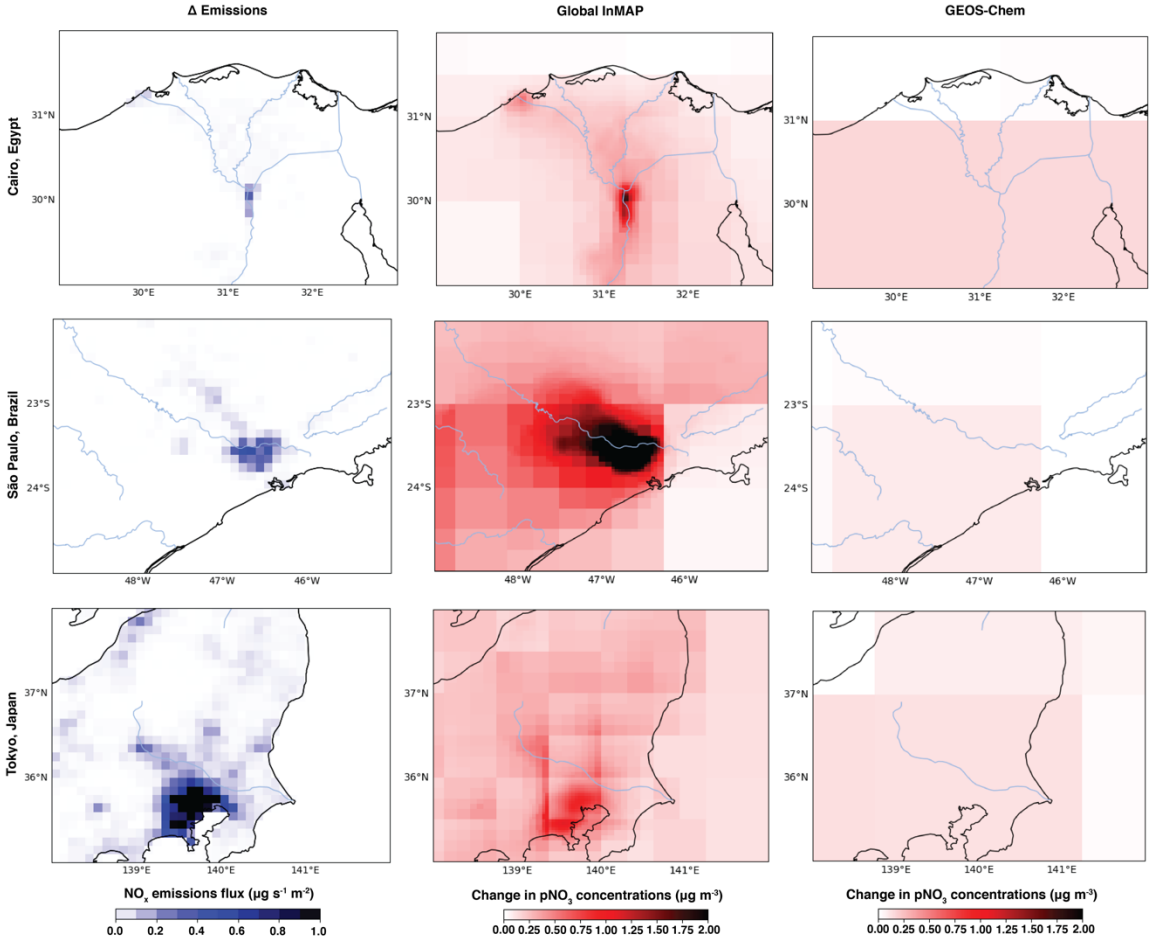

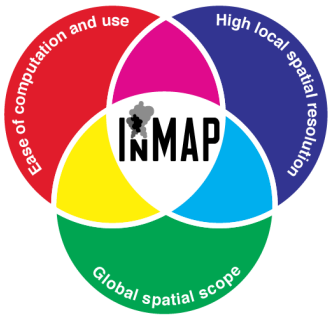

For Table of Contents Use Only.

Global, high-resolution reduced-complexity air quality modeling using InMAP (Intervention Model for Air Pollution)

Sumil K. Thakrar, Christopher W. Tessum, Joshua S. Apte, Srinidhi Balasubramanian, Dylan B. Millet, Spyros N. Pandis, Julian D. Marshall, Jason D. Hill.

Global, high-resolution, reduced-complexity air quality modeling using InMAP (Intervention Model for Air Pollution)

Sumil K. Thakrar[1,2], Christopher W. Tessum[3], Joshua S. Apte[4,5], Srinidhi Balasubramanian[1], Dylan B. Millet[6], Spyros N. Pandis[7,8], Julian D. Marshall[9], Jason D. Hill[1*].

[1]Department of Bioproducts & Biosystems Engineering, University of Minnesota, St Paul, MN, USA.

[2]Department of Applied Economics, University of Minnesota, St Paul, MN, USA.

[3]Department of Civil and Environmental Engineering, University of Illinois at Urbana–Champaign, Urbana, IL, USA.

[4]Department of Civil and Environmental Engineering, University of California, Berkeley, Berkeley, CA, USA.

[5]School of Public Health, University of California, Berkeley, Berkeley, CA, USA.

[6]Department of Soil, Water, and Climate, University of Minnesota, St Paul, MN, USA.

[7]Department of Chemical Engineering, Carnegie Mellon University, Pittsburgh, PA, USA.

[8]Department of Chemical Engineering, University of Patras, Greece.

[9]Department of Civil and Environmental Engineering, University of Washington, Seattle, WA, USA.

Corresponding author: Jason D. Hill
Email: hill0408@umn.edu

Supplementary Information Text

Measurement data description

Ground-level measurements of total $PM_{2.5}$, pNH_4, pNO_3, and pSO_4 concentrations across year 2016 were compiled from the World Health Organization database and supplemented with additional measurements from other official channels such as governmental and non-governmental agencies (see Table S2). Included measurements were vetted according to quality control criteria, including those used by the 2012 United States National Ambient Air Quality Standards. Only measurements that directly measured $PM_{2.5}$ were included; PM_{10} measurements that were converted to $PM_{2.5}$ were excluded. Further, data without correct latitude and longitude were excluded. Global InMAP directly estimates annual-average pollutant concentrations, so measurement data from each monitoring site were averaged across the year. To avoid temporal biases across the day, all measurement data were averaged daily values of pollutant concentrations. To avoid seasonal biases, measurements had to be reported for at least 75% of days in the year from each monitoring site included in our dataset.

After vetting, the final dataset of annual-average pollutant concentrations included ~1,700 total $PM_{2.5}$ data points across 62 countries; 171 pNH_4 data points across 1 country (the US); 334 pNO_3 data points across 4 countries, and 385 pSO_4 data points across 12 countries. The final dataset is provided in Dataset S1.

Performance metric and criteria descriptions

Normalized mean bias and error (NMB and NME), are given by:

$$NMB = \frac{\sum_i P_i - O_i}{\sum_i O_i} \times 100$$

$$NME = \frac{\sum_i |P_i - O_i|}{\sum_i O_i} \times 100$$

where, for monitor location i, P_i are the model predictions and O_i are the observations of annual-average pollutant concentrations.

Model criteria for $PM_{2.5}$, pSO_4, and pNH_4 concentrations, are $R^2 \geq 0.16$, NME ≤ 50%, and |NMB| ≤ 30%. For pNO_3, model criteria are NME ≤ 115%, |NMB| ≤ 65% (with no criteria for R^2).

For model-to-model comparisons, weighted NMB and NME are given by:

$$NMB_{weighted} = \frac{\sum_i (GI_i - M_i) \times w_i}{\sum_i O_i \times w_i} \times 100$$

$$NME_{weighted} = \frac{\sum_i |GI_i - M_i| \times w_i}{\sum_i M_i \times w_i} \times 100$$

Where w_i are the weights (areas or population counts) for each grid cell i, GI are the Global InMAP predictions, and M are the predictions from the other model (GEOS-Chem or US InMAP).

Supplementary Figure 1. Detail of the Global InMAP horizontal computational grid over West Africa, Central America, and Europe for illustration. Grid cells are as small as 0.04° × 0.03° (~4 km length) in areas with a higher population such as Lagos in Nigeria, San Salvador in El Salvador, and London in the United Kingdom. Grid cells are as large as 5° × 4° (~500 km length) in places with a lower population, such as across the Atlantic Ocean.

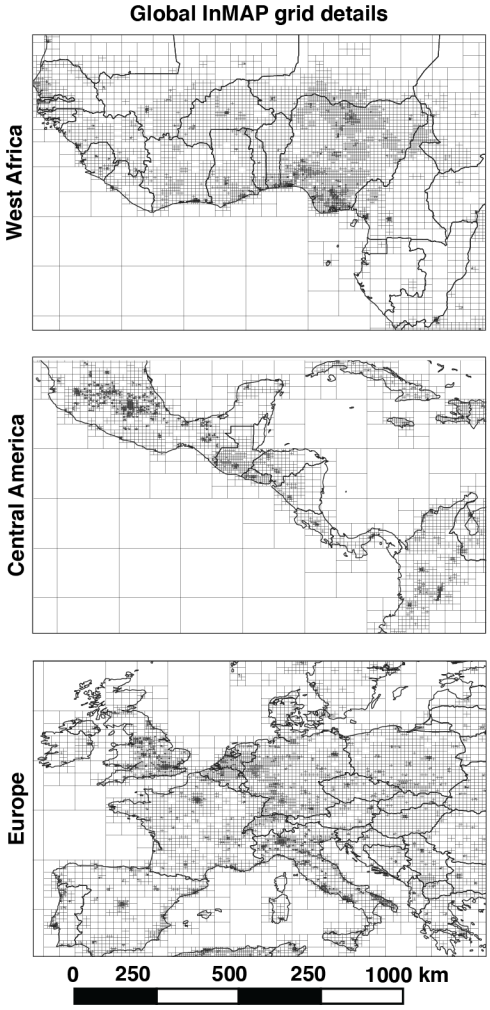

Supplementary Figure 2. InMAP and GEOS-Chem annual-average primary $PM_{2.5}$ concentrations against measurements, including outliers (above 100 μg m^{-3}).

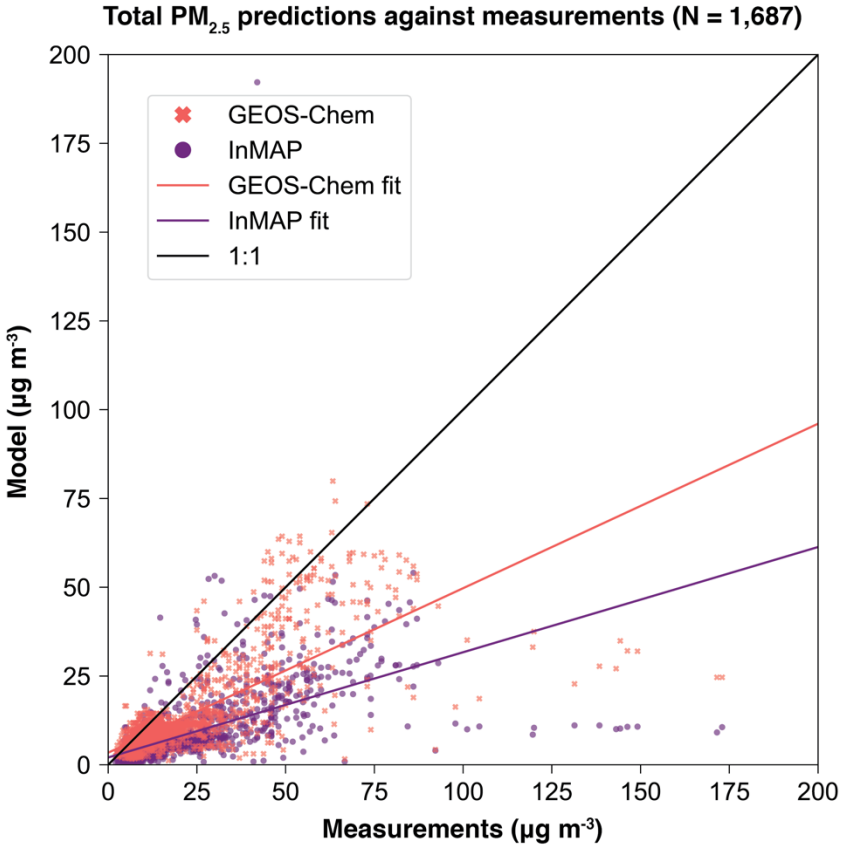

	NMB	NME	Slope	R^2
GEOS-Chem	-37%	41%	0.46	0.55
Global InMAP	-60%	63%	0.30	0.35

Supplementary Figure 3. Performance of Global InMAP and GEOS-Chem simulations against total annual-average $PM_{2.5}$ measurements for Africa. Dots on each map show measurement site locations, whose color corresponds to the model-measurement difference in $PM_{2.5}$ concentrations.

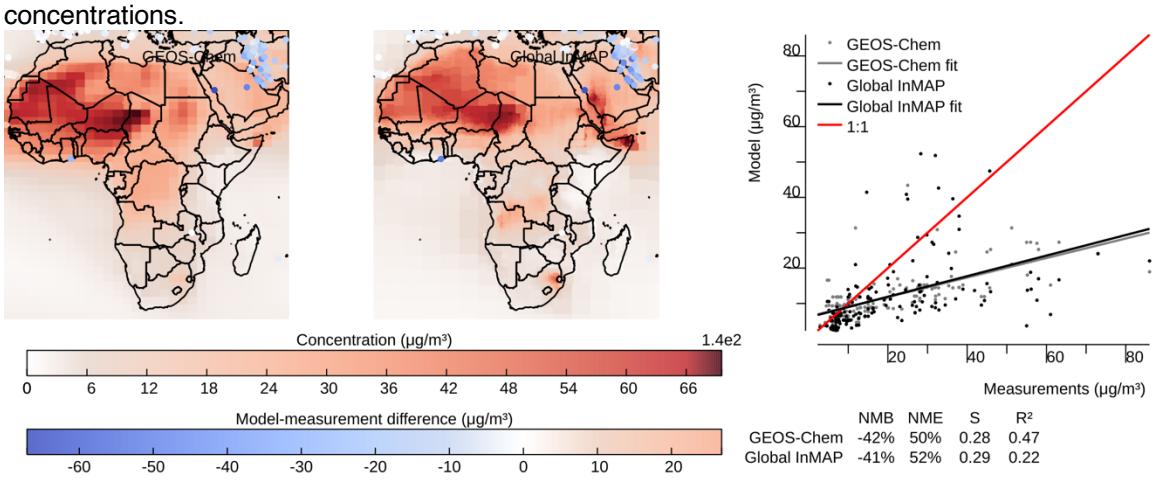

	NMB	NME	S	R^2
GEOS-Chem	-42%	50%	0.28	0.47
Global InMAP	-41%	52%	0.29	0.22

Supplementary Figure 4. Performance of Global InMAP and GEOS-Chem simulations against total annual-average $PM_{2.5}$ measurements for Asia. Dots on each map show measurement site locations, whose color corresponds to the model-measurement difference in $PM_{2.5}$ concentrations.

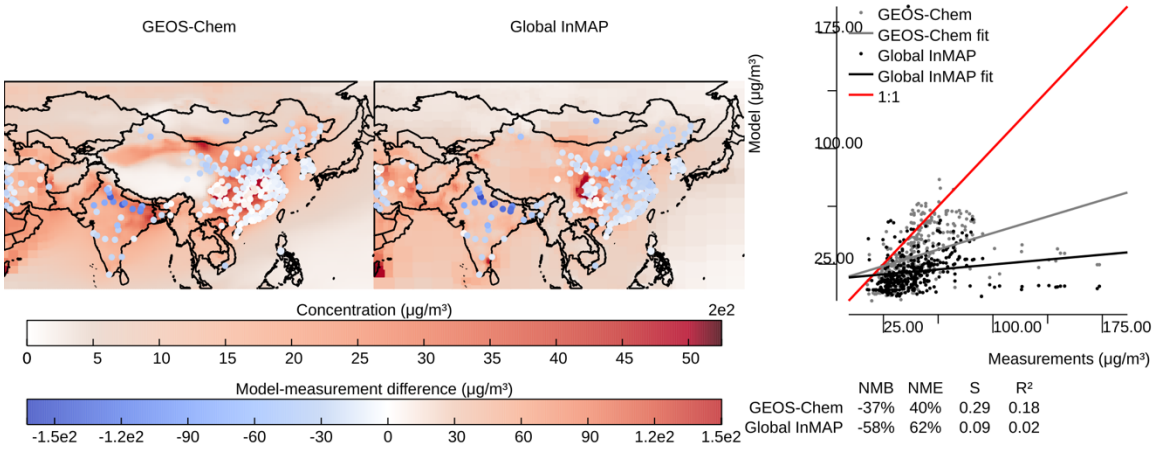

	NMB	NME	S	R^2
GEOS-Chem	-37%	40%	0.29	0.18
Global InMAP	-58%	62%	0.09	0.02

Supplementary Figure 5. Performance of Global InMAP and GEOS-Chem simulations against total annual-average $PM_{2.5}$ measurements for Europe. Dots on each map show measurement site locations, whose color corresponds to the model-measurement difference in $PM_{2.5}$ concentrations.

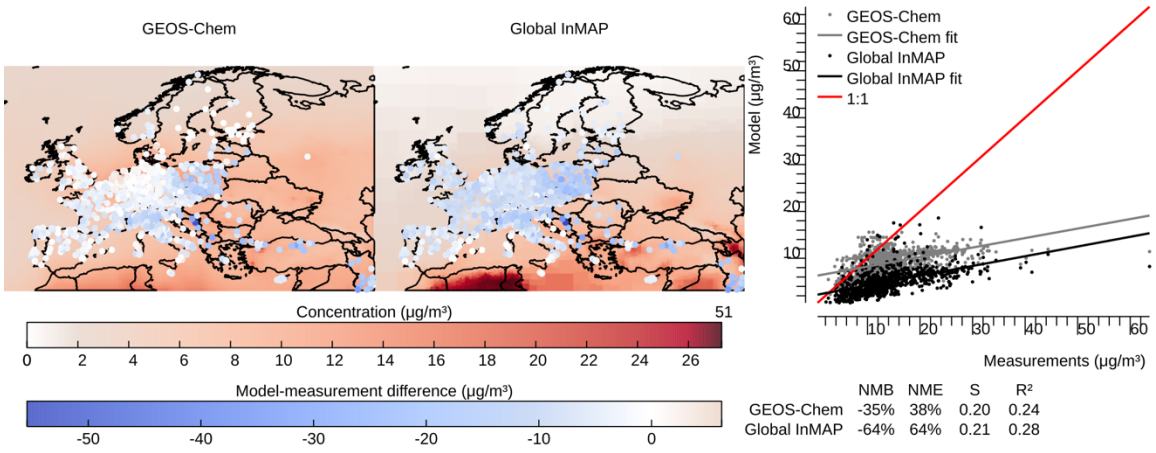

	NMB	NME	S	R^2
GEOS-Chem	-35%	38%	0.20	0.24
Global InMAP	-64%	64%	0.21	0.28

Supplementary Figure 6. Performance of Global InMAP and GEOS-Chem simulations against total annual-average $PM_{2.5}$ measurements for North and Central America. Dots on each map show measurement site locations, whose color corresponds to the model-measurement difference in $PM_{2.5}$ concentrations.

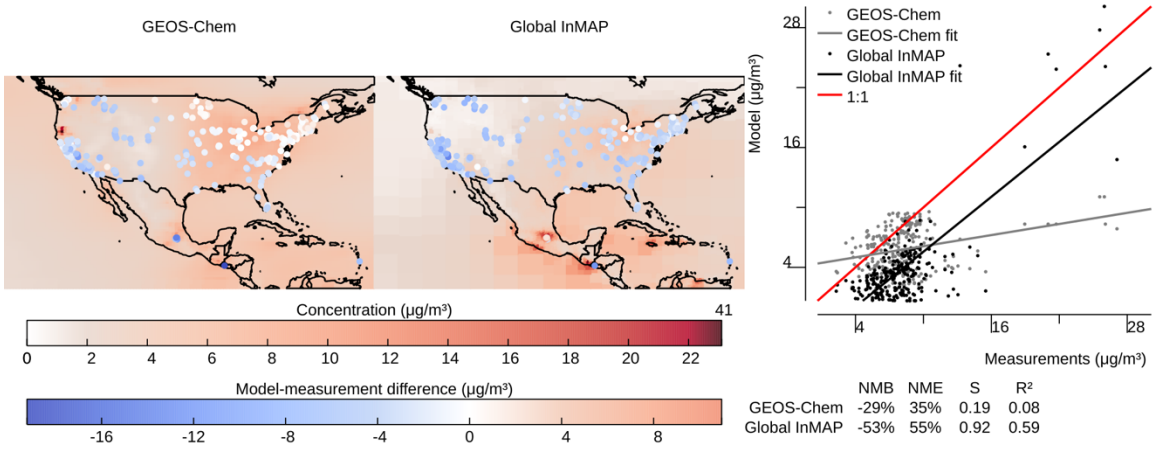

	NMB	NME	S	R^2
GEOS-Chem	-29%	35%	0.19	0.08
Global InMAP	-53%	55%	0.92	0.59

Supplementary Figure 7. Performance of Global InMAP and GEOS-Chem simulations against total annual-average $PM_{2.5}$ measurements for Oceana. Dots on each map show measurement site locations, whose color corresponds to the model-measurement difference in $PM_{2.5}$ concentrations.

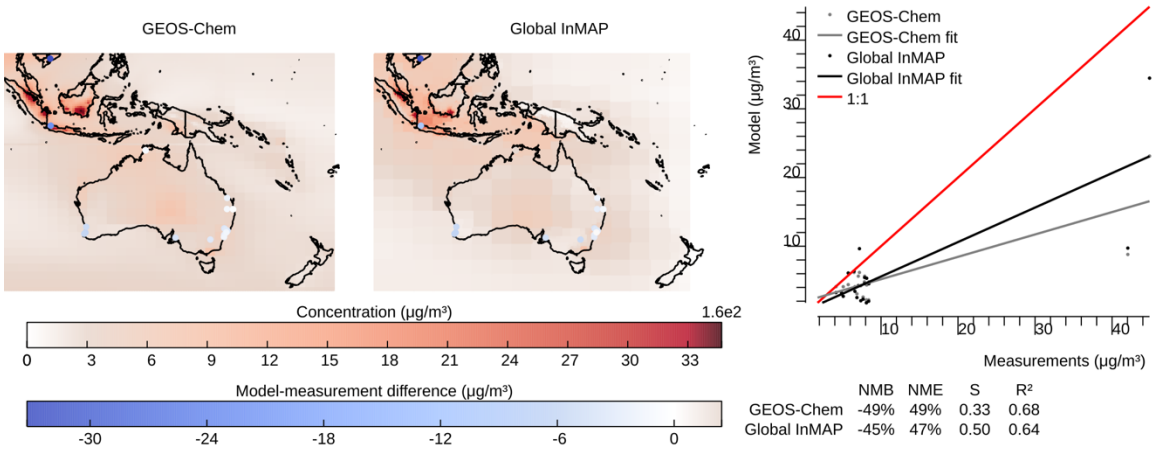

	NMB	NME	S	R^2
GEOS-Chem	-49%	49%	0.33	0.68
Global InMAP	-45%	47%	0.50	0.64

Supplementary Figure 8. Performance of Global InMAP and GEOS-Chem simulations against total annual-average $PM_{2.5}$ measurements for South America. Dots on each map show measurement site locations, whose color corresponds to the model-measurement difference in $PM_{2.5}$ concentrations.

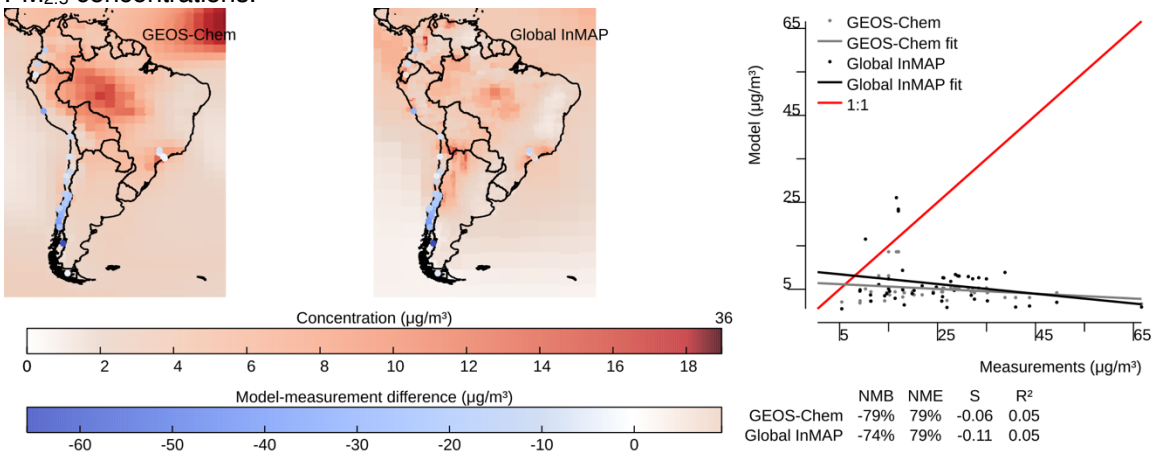

	NMB	NME	S	R^2
GEOS-Chem	-79%	79%	-0.06	0.05
Global InMAP	-74%	79%	-0.11	0.05

Supplementary Figure 9. Changes in Total $PM_{2.5}$ concentrations from road vehicle emissions and from power generation emissions as predicted by Global InMAP (which has GEOS-Chem preprocessor inputs) alongside US InMAP (which has WRF-Chem preprocessor inputs).

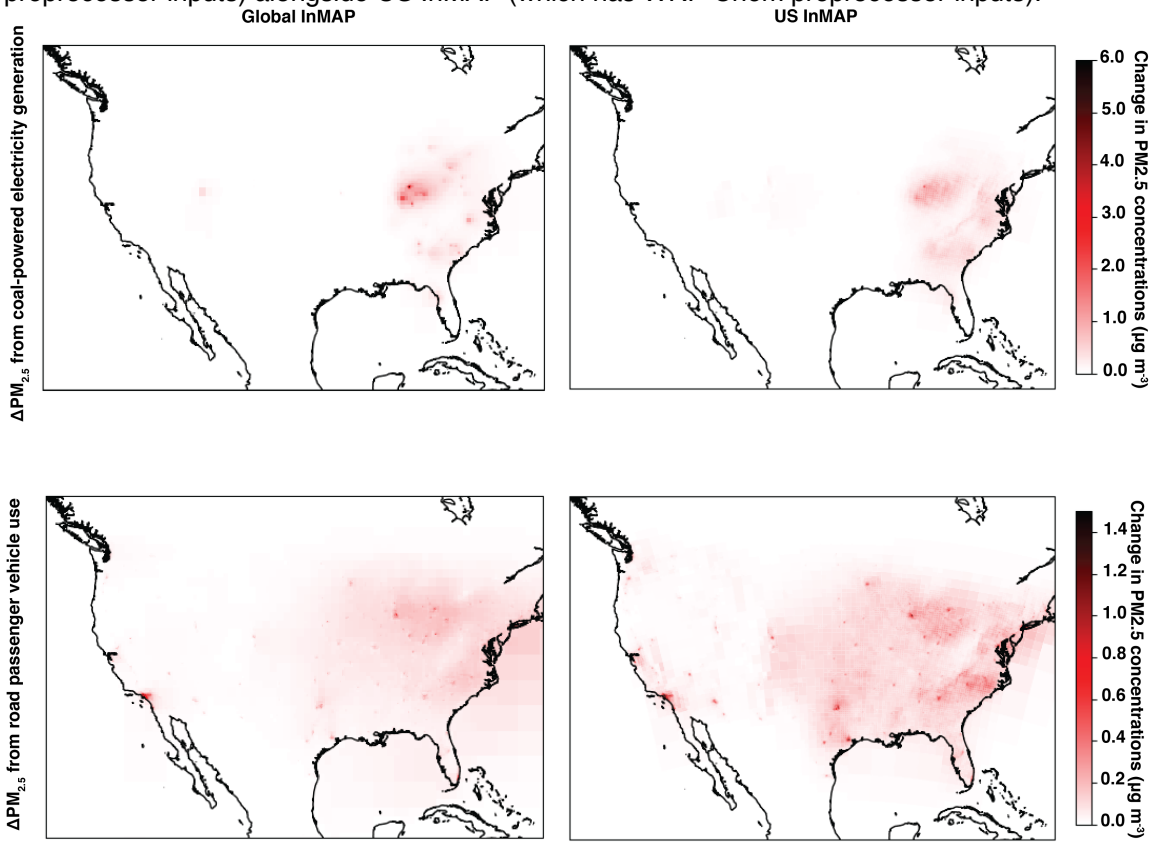

Supplementary Table 1. Names and descriptions of GEOS-Chem outputs used to calculate Global InMAP parameters.

Name(s)	Description and use in Global InMAP preprocessor
BENZ, TOLU, XYLE, NAP, POG1, POG2	Anthropogenic VOCs that are SOA precursors; used to determine VOC/SOA partitioning
ASOA1, ASOA2, ASOA3, ASOAN	Anthropogenic SOA; used to determine VOC/SOA partitioning
ISOP, LIMO, MTPA, MTPO	Biogenic VOCs that are SOA precursors; used for model evaluation
TSOA0, TSOA1, TSOA2, TSOA3, SOAGX, SOAMG, SOAIE, SOAME, LVOCOA, ISN1OA	Biogenic SOA; used for model evaluation
NO, NO2	Components of NO_x; used to determine NO_x /pNO_3 partitioning
NIT, NITs	Components of pNO_3; used to determine NO_x /pNO_3 partitioning
SO2	Gaseous SO_2 and sulfate; used to determine SO_x /pSO_4 partitioning
SO4, SO4s, DMS	Particulate SO_4; used to determine SO_x /pSO_4 partitioning
NH3	Ammonia; used to determine NH_3/pNH_4 partitioning
NH4	Particulate Ammonium; used to determine NH_3/pNH_4 partitioning
1.33×(NH4 + NIT + SO4) + BCPI + BCPO + 1.4×(POA1 + POA2) + 2.1×(OPOA1 + OPOA2) + 1.16×(TSOA1 + TSOA2 + TSOA3 + ASOAN + ASOA1 + ASOA2 + ASOA3 + SOAGX + INDIOL + SOAMG + SOAIE + SOAME + LVOCOA + ISN1OA) + DST1 + 0.38×DST2 + 1.86×SALA	Total $PM_{2.5}$ concentration in the baseline simulation; used for model evaluation
Z0M	Momentum roughness length
U, V, OMEGA	Wind fields; used to determine advection and mixing coefficients
PBLH	Planetary boundary layer height; used to determine mixing coefficients
HFLUX	Surface heat flux; used to determine mixing and dry deposition
USTAR	Friction velocity; used to determine mixing and dry deposition
T	Temperature; used to calculate chemical reaction rates and plume rise
PS, P	Base state pressure plus perturbation pressure; used to calculate chemical reaction rates and plume rise
OH, H2O2	Hydroxyl radical and hydrogen peroxide concentrations; used to calculate chemical reaction rates
FRSNO	Fraction of land covered by snow; used to calculate dry deposition

PFLCU, PFLLSAN	Mixing ratio of rain; used to calculate wet deposition
CLOUD	Fraction of grid cell covered by clouds; used to calculate wet deposition
QL	Cloud mixing ratio; used to calculate aqueous-phase chemical reaction rates
AIRDEN	Inverse air density; used to calculate mixing and to convert between mixing ratio and mass concentration
PARDF, PARDR	Downward shortwave and longwave radiative flux at ground level; used to calculate dry deposition

Supplementary Table 2. Measurement data sources for 2016 used in evaluating Global InMAP and GEOS-Chem annual-average predictions of pollutant concentrations. The World Health Organization data includes data from other regulatory sources and monitoring networks globally.

Region	Data	Source
Global	$PM_{2.5}$	World Health Organization
Europe	$PM_{2.5}$, pNO_3, pSO_4	European Environment Agency
Canada	$PM_{2.5}$	National Air Pollution Surveillance Program
United States of America	$PM_{2.5}$, pNO_3, pSO_4, pNH_4	Environmental Protection Agency
India	$PM_{2.5}$	Central Pollution Control Board
Australia	$PM_{2.5}$	Australian Government State of the Environment

Supplementary Table 3. Global InMAP and GEOS-Chem performance metrics for total $PM_{2.5}$ concentrations globally, speciated $PM_{2.5}$ concentrations globally, and total $PM_{2.5}$ concentrations regionally. Bold values do not meet the performance criteria (see Supplementary Text). NMB: normalized mean bias (%); NME: normalized mean error (%).

	Global InMAP			GEOS-Chem		
	NMB (%)	NME (%)	R^2	NMB (%)	NME (%)	R^2
Total $PM_{2.5}$	**-60**	**63**	0.35	**-37**	41	0.55
pSO_4	48	**67**	0.38	18	37	0.42
pNO_3	-24	50	0.24	-12	53	0.25
pNH_4	35	**65**	0.24	**79**	**110**	**0.08**
Africa	**-41**	**52**	0.22	**-42**	50	0.47
Asia	**-58**	**62**	**0.02**	**-37**	40	0.18
Europe	**-64**	**64**	0.28	**-35**	38	0.24
North & Central America	**-53**	**55**	0.59	-29	35	**0.08**
Oceana	**-45**	**47**	0.64	**-49**	**49**	0.68
South America	**-74**	**79**	**0.05**	**-79**	**79**	**0.05**

Dataset S1 (Online at doi.org/10.5281/zenodo.4641947). Input data (including population, grid, and emissions data) used to perform and evaluate Global InMAP simulations.